

# Face-Off: Adversarial Face Obfuscation

Chuhan Gao<sup>\*†</sup>, Varun Chandrasekaran<sup>\*†</sup>, Kassem Fawaz<sup>\*</sup>, Somesh Jha<sup>\*</sup>

University of Wisconsin-Madison<sup>\*</sup>, Equal Contribution<sup>†</sup>

**Abstract**—Advances in deep learning have made face recognition increasingly feasible and pervasive. While useful to social media platforms and users, this technology carries significant privacy threats. Coupled with the abundant information they have about users, service providers can associate users with social interactions, visited places, activities, and preferences - some of which the user may not want to share. Additionally, facial recognition models used by various agencies are trained by data scraped from social media platforms. Existing approaches to mitigate these privacy risks from unwanted face recognition result in an imbalanced privacy-utility trade-off to the users. In this paper, we address this trade-off by proposing Face-Off, a privacy-preserving framework that introduces minor perturbations to the user’s face to prevent it from being correctly recognized. To realize Face-Off, we overcome a set of challenges related to the black box nature of commercial face recognition services, and the lack literature for adversarial attacks on metric networks. We implement and evaluate Face-Off to find that it deceives three commercial face recognition services from Microsoft, Amazon, and Face++. Our user study with 330 participants further shows that the perturbations come at an acceptable cost for the users.

## I. INTRODUCTION

Enabled by advances in deep learning, face recognition is becoming increasingly pervasive in several contexts, such as social media, online photo storage applications, and law enforcement [31]. Companies such as Facebook, Google, and Amazon provide their users various services built atop face recognition, including automatic tagging and grouping of faces. Users share their photos with these platforms, which then (a) detect (through semantic segmentation) and (b) recognize the faces present in these photos. These forms of automated recognition, however, pose privacy threats to users, induce bias, and violate legal frameworks [1], [31]. These organizations operate black box recognition and segmentation models that allow for associating users with social interactions, visited places, activities, and preferences - some of which the user may not want to share.

Existing approaches to mitigate these privacy risks from unwanted identification result in an imbalanced privacy-utility trade-off to the users. These solutions rely on (a) blurring/obscuring/morphing faces [10], (b) having the users utilize physical objects, such as eyeglass frames with special patterns, clothes worn by the user, scenery around the user, etc. [26], [27], and (c) evading face detection by dodging the face detector [4]. These solutions, however, exhibit two main drawbacks: (a) the user is no longer able to meet her original goal in using the social media platform, especially when various applications built atop of face detection, such as face-enhancement features, are broken, and (b) specially manufactured physical obfuscation objects are not omnipresent.

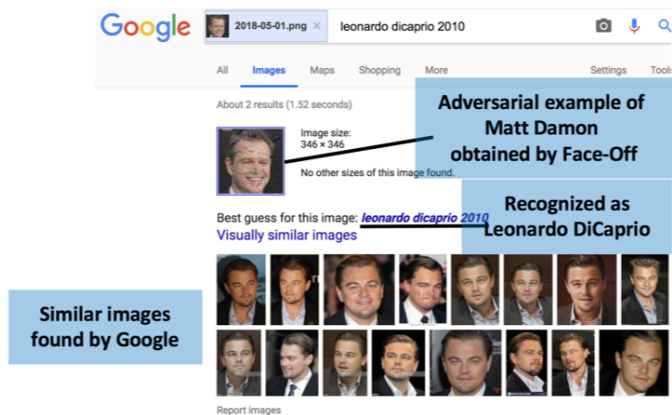


Fig. 1: Adversarial example of Matt Damon generated by Face-Off recognized as Leonardo DiCaprio by Google image search.

Relying on insights from previous work [26], [27], [4], we propose a new paradigm to improve the trade-off between privacy and utility for such users. In adversarial machine learning, carefully crafted images result in small and human-imperceptible perturbations that cause misclassifications [29], [9], [6]. In this paper, we extend this approach from classification models to the recognition/verification domain. In particular, we propose Face-Off, a privacy-preserving adversarial attack scheme against *real-world* face recognition systems. By carefully designing the adversarial perturbation, Face-Off targets only face recognition (and not face detection), preserving the user’s original intention along with context associated with the image. Face-Off detects a user’s face(s) from an image to-be-uploaded, applies the necessary adversarial perturbation on the face, and returns the image with a perturbed face. The objective of Face-Off is to allow a service provider to detect faces in the image but prevent it from attributing the image to the correct person. Meanwhile, the perturbation should be kept at a minimal level.

In the course of realizing Face-Off, we face the following challenges:

- Unlike classifiers face verification/recognition networks are metric learning systems that aim at representing each input as a feature embedding [25], [30], [15]. Real-world face recognition takes place by mapping the feature embedding to the closest cluster of faces. Existing adversarial attacks only focus on classifiers, and must be retrofit for verification networks.
- As the models used by these organizations are proprietary,

Face-Off needs to perform *black box attacks*. This is known to be difficult in the classifier domain [29], [6], [21]. Further, Face-Off cannot use the service provider’s face recognition API as a black box oracle to generate the adversarially perturbed face [26] for two reasons. First, generating an adversarial example requires querying the API extensively, which is not free and is often rate-limited. Second, querying the black box model defeats our purpose for privacy protection as it sometimes begins with releasing the original face [26].

We address the first challenge by designing two new loss functions for the adversarial attack specifically targeting metric learning systems. These loss functions aim to pull the input face away from a cluster of faces belonging to the user (in the embedding space), which results in incorrect face recognition. Both loss functions can be integrated with the state-of-the-art adversarial attacks against classifiers [6], [17], thereby providing the additional benefit of being compatible with advances in adversarial attack schemes for classifiers.

To meet the second challenge, we leverage the property of *transferability*, where an adversarial example generated for one model is also adversarial for another. We rely on substitute face recognition models which we have full access to generate adversarial examples. After perturbing the face using these substitute models, Face-Off amplifies the perturbation by a small multiplicative factor  $\alpha$  as to enhance transferability. This property ensures that verification networks will not recognize our perturbed faces. Amplification has been shown to improve the robustness of adversarial examples for classifiers [5]. In this paper, we further explore amplification and show it enhances transferability in metric networks and reduces the time required to generate an adversarial example.

Apart from the aforementioned loss function, Face-Off is a framework that incorporates two other components: a white box model serving as substitute model and an adversarial attack algorithm. In our implementation, we use two recently proposed and high accuracy face recognition models [25], [36] as white box models. For the attack algorithm, Face-Off utilizes the Carlini & Wagner [6] and the projected gradient descent [17] attacks - two of the latest and most effective adversarial example generation strategies. Users of Face-Off can vary different parameters associated with its components to determine their desired trade-off between privacy gains, the utility of the image, and execution time.

We evaluate Face-Off using a set of celebrity photos across three major commercial face recognition services: Microsoft Azure Face API <sup>1</sup>, AWS Rekognition <sup>2</sup>, and Face++ <sup>3</sup>. Face-Off generates images, with low perturbation, that transfer to these three services. After applying sufficient amplification, Face-Off achieves nearly 100% privacy protection by preventing all three services from correctly recognizing the input face. Our adversarial examples also transfer to Google image search (Fig.

1) successfully with the target labels. Finally, we perform a user study on Amazon Mechanical Turk with 330 participants to evaluate user perception of the perturbed faces. Through our user studies, we determine that the degree of perturbation in the images that transfer is acceptable to end-users; privacy-conscious users are willing to tolerate greater perturbation levels for improved privacy.

In summary, we offer the following contributions in this paper:

- 1) We design a set of loss functions that target adversarial examples for metric networks (§ IV). We also highlight how amplification improves transferability across both metric (§ V) and classification networks (§ VII).
- 2) We design, implement and evaluate Face-Off, which applies adversarial perturbation to prevent real-world face recognition platforms from correctly tagging user’s face (§ VIII). We confirm Face-Off’s capabilities across three major commercial face recognition services: Microsoft Azure Face API, AWS Rekognition, and Face++.
- 3) We perform a user study (including 330 participants) to assess the user-perceived utility of the images that Face-Off generates (§ VI).

## II. BACKGROUND

### A. Face Recognition

State-of-the-art face recognition platforms utilize verification models. The model takes a pair of faces as inputs and performs some form of matching to determine if these two faces belong to the same individual. To do so, the verification model generates a fixed length embedding for each input image and compares the distance between embeddings. The networks used for this purpose are sometimes called Siamese networks [25], [36], and this type of learning is referred to as metric embedding or metric learning [39], [35]. Compared to classification, verification can scale to an arbitrary number of identities. As a result, modern applications tend to resort to verification for face recognition tasks <sup>45</sup>. Throughout this paper, face recognition refers exclusively to face verification. Due to the fundamental different working principle of face verification, the model inference and training processes differ from conventional classifiers; below, we provide a brief introduction.

**Architectures:** A standard classification model employs a deep neural network  $F_\theta$ , where  $\theta$  represents the model parameters. For an input  $x \in \mathbb{R}^m$ , the network generates  $y = F_\theta(x)$ . Typically, the last layer of the network employs a softmax function which generates the probability distribution  $y \in \mathbb{R}^n$ . Here,  $y_i$  represents the probability of the input  $x$  belonging to class  $i$ .

On the other hand, a verification model consists of *two identical feedforward networks* -  $F_\theta^1$  and  $F_\theta^2$ . For a pair of input faces  $x_1, x_2 \in \mathbb{R}^m$ , each sister network produces a fixed length feature vector  $Z_i = F_\theta^i(x_i)$  for  $i = 1, 2$  respectively. We

<sup>1</sup><https://azure.microsoft.com/en-us/services/cognitive-services/face/>

<sup>2</sup><https://aws.amazon.com/rekognition/>

<sup>3</sup><https://www.faceplusplus.com/>

<sup>4</sup>How does Facebook’s face recognition work? <https://www.facebook.com/help/122175507864081>

<sup>5</sup>Google Photos Face Grouping. <https://support.google.com/photos/answer/6128838?co=GENIE.Platform%3DAndroid&hl=en>

refer to this feature vector as the *embedding* of the input face [25]. The last layer of the Siamese network computes the distance (typically  $\ell_2$ -norm) between embedding  $Z_1$  and  $Z_2$ , which is then used for verification. In the remainder of this paper, we refer to this distance as the *feature distance*.

**Loss Functions:** Unlike classification models that supervise the training process with loss functions such as cross-entropy loss, training verification models requires different functions. These include contrastive loss [7], [11] and triplet loss [25], [34], [8]. Recent approaches in face recognition explore new loss functions to improve performance. For example, using center loss [36], the neural network is trained to cluster embedding of samples with the same identity closely around a centroid. Another example is angular-softmax loss [15], which imposes discriminative constraints on a hypersphere manifold.

### B. Adversarial Examples

While neural networks represent the state-of-the-art for various classification tasks, they are vulnerable to a variety of adversarial attacks [22], [38]. It is possible to misclassify input images with carefully crafted, human-imperceptible perturbations [29]. These *adversarial examples* can also cause (adversary-chosen) targeted misclassification. While some defenses exist, they are shown to be at tension with utility [17].

**Adversarial Example Generation:** For a given input  $x \in \mathbb{R}^n$ , recall that  $y = F_\theta(x)$  denotes the probability distribution of the outputs. An adversarial example  $x' = x + \delta$  is one such that  $\arg \max_i F_\theta(x) \neq \arg \max_i F_\theta(x')$ , where  $c = \arg \max_i y$  denotes the label of the most probable classification output. The problem of determining the perturbation  $\delta$  is typically modeled as a constraint optimization problem, with the objective of minimizing the  $p$ -norm of perturbation:

$$\begin{aligned} & \text{minimize} && \|\delta\|_p \\ & \text{subject to} && \arg \max_i F_\theta(x) \neq \arg \max_i F_\theta(x') \text{ (untargeted)} \\ & \text{OR} && \\ & \text{subject to} && \arg \max_i F_\theta(x') = t \text{ (targeted)} \end{aligned}$$

where  $t$  is an attacker chosen label. As the above optimization problem is hard to solve in practice, different practical solutions have been proposed. We refer the curious reader to solutions by Carlini and Wagner [6] (henceforth referred to as CW), and Madry *et al.* [17] (henceforth referred to as PGD).

## III. SYSTEM OVERVIEW

In the following section, we present the threat model we consider, as well as a high-level overview of Face-Off.

### A. System and Threat Models

A user takes a photo and shares it on a social media platform (such as Facebook or Instagram). The online platform first utilizes a *face detector* to identify the faces in the photo, and then applies *face recognition* to tag the faces. Once each photo has been indexed by the set of people appearing in it, the platform can perform additional inferences about the behavior

of people, places they visit, activities they engage in, and their social circles [1]. Additionally, these photos can be scraped by various services, and later used by various governmental agencies [31]. Thus, we assume the platform to be an “honest-but-curious” entity. This prolonged analysis of user photos allows the platform (and other agencies that use these photos) to profile users. This in turn enables targeted advertising, and potentially monitoring and surveillance at the behest of a nation-state. We characterize the social media platform as follows:

1. It uses proprietary black box model(s) for face recognition.
2. The users upload images of various sizes, resolutions, and formats to the platform. The platform successfully (or with high probability) recognizes faces in all of them.

### B. High Level Overview of Face-Off

To prevent the platform from recognizing a user’s face, we design Face-Off, a tool that generates perturbations that induce failures. At a high level, Face-Off operates as follows (Fig. 2):

- 1) Receives the desired image from the user.
- 2) Detects and extracts faces.
- 3) Resizes the faces as required by the adversarial example generation pipeline (refer § IV-B).
- 4) Generates perturbation for the faces.
- 5) Returns a perturbed image of the original size (to upload).

We envision two deployment models of Face-Off.

**1. Trusted Cloud:** Face-Off’s GPU-powered cloud service receives detected faces from the client on the user’s machine. It applies the necessary perturbation and returns the perturbed images for the user. Note that the cloud service only receives low-resolution faces (which are detected and cropped locally) to generate the adversarial perturbation. With the input face, Face-Off requires additional information of limited size, which we elaborate in § VIII-G. Face-Off resizes, amplifies, and applies the perturbation to the image locally.

**2. Local Deployment:** While the former approach involves trusting the cloud, the local deployment can perform all operations locally at the client.

In § VIII-G, we evaluate the running time of both these deployment models.

### C. Challenges

Achieving the aforementioned functionality is challenging. We highlight several reasons below:

- C1. Verification based architectures use a different loss function (as described in § II) than those used in existing work on adversarial example generation. New loss functions are to be designed to bridge the gap.
- C2. The models used by the platform are black box.
- C3. Our attacks utilize substitute models that mirror the black box models to *only some* degree. Thus, the generated adversarial examples *must* transfer.
- C4. Since Face-Off resizes the images, it is essential that the perturbation generated for the scaled image transfers as well, as it is resized and potentially compressed.

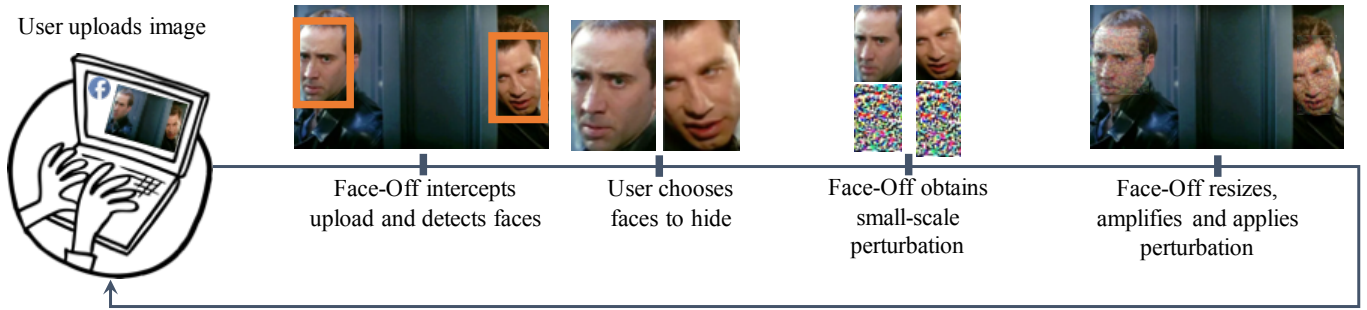


Fig. 2: High-level overview of Face-Off's processing pipeline.

#### IV. SYSTEM DESIGN

In this section, we first present our white box attack, and then describe how we tweak the adversarial example to improve transferability to black box models.

##### A. Attacks on Substitute Models

Our optimization is similar to that of Carlini *et al.* [6]:

$$\begin{aligned} & \underset{\delta}{\text{minimize}} && \|\delta\|_p + c \cdot \mathcal{L}(x + \delta) \\ & \text{subject to} && x + \delta \in [0, 1] \end{aligned}$$

where  $\mathcal{L}(x + \delta)$  is a loss function that reflects the success of the attack.  $c$  is a parameter, determining the weight of the loss function with respect to the amplitude of perturbation.

**Customized Loss Functions:** To ensure that the attack is successful for metric learning, we introduce:

1. *Target loss* is defined as the feature distance between the adversarial example and a set of faces with a target label  $t$ . This can be expressed as

$$\mathcal{L}_t(x + \delta) = \left\| F_\theta(x + \delta) - \frac{1}{N} \sum_{j=1}^N F_\theta(x^{j,t}) \right\|_2,$$

where  $x^{m,n}$  denotes the  $m^{\text{th}}$  sample with label  $n$ ,  $N$  is the total number of instances ( $x^{j,t}$ ). We refer to  $N$  as the batch size.

2. *Hinge loss* simultaneously maximizes the feature distance between the adversarial example and the original image (with label  $o$ ), in addition to what target loss achieves.

$$\begin{aligned} \mathcal{L}_h(x + \delta) &= \max(A - B + \kappa, 0) \\ A &= \left\| F_\theta(x + \delta) - \frac{1}{N} \sum_{j=1}^N F_\theta(x^{j,t}) \right\|_2 \\ B &= \left\| F_\theta(x + \delta) - \frac{1}{N} \sum_{j=1}^N F_\theta(x^{j,o}) \right\|_2 \end{aligned}$$

When minimizing hinge loss, we use a parameter  $\kappa$  to control the desired *margin* of the feature distance. Specifically, we want the distance between the adversarial example and the original instance (denoted by the term  $B$ ) to be larger than the distance between the adversarial example and the target instance

(denoted by the term  $A$ ) by a certain amount. Achieving a larger margin is equivalent to pushing the adversarial example further into the decision space of the target label, which is likely to improve transferability (refer § V).

Observe that minimizing the two loss functions amounts to moving the adversarial image towards another (target) identity in the embedding space. Given these loss functions (which satisfy **C1**), we utilize a substitute network (which satisfies **C2**) of known architecture and parameters (which we elaborate in § VIII) to generate the desired adversarial example.

##### B. Black Box Attacks

We utilize the property of *transferability* to enable attacks generated on known models to transfer to black-box models [33]. This simple, yet powerful property has been demonstrated extensively in prior work [6], [16], [32], [19].

We perform offline analysis to determine the best set of parameters to use to minimize computational overhead. The adversarial example generated using these parameters is then *amplified* using a small multiplicative factor; while nominal amplification does not impact discernibility, it improves transferability (which satisfies **C3**). Evidences of amplification exist in previous work [5] to strengthen the adversarial example. To the best of our knowledge, we are the first to investigate its utility in enhancing transferability.

Recall that the face is cropped and *resized* before being perturbed. Since this size is not appropriate to return to the user, we resize the resulting perturbed image back to the original size. We observe that the resizing preserves transferability (which satisfies **C4**). We hypothesize this to be the case because black box APIs will resize the images as we do to perform face recognition, consequently preserving the perturbation we generate. We evaluate this hypothesis in § VIII.

#### V. LIPSCHITZ CONTINUITY

**Theoretical Intuition:** Let  $f$  be function from  $\mathbb{R}^n$  to  $\mathbb{R}^m$  where  $n \gg m$ . For example,  $\mathbb{R}^n$  could denote the image space and  $\mathbb{R}^m$  could denote the embedding space. Given a closed and compact sub-space  $S \subseteq \mathbb{R}^n$ , we define the Lipschitz constant [2]  $L_f(S)$  as

$$\sup \left\{ \frac{\|f(x) - f(y)\|}{\|x - y\|} : x, y \in S \right\}$$

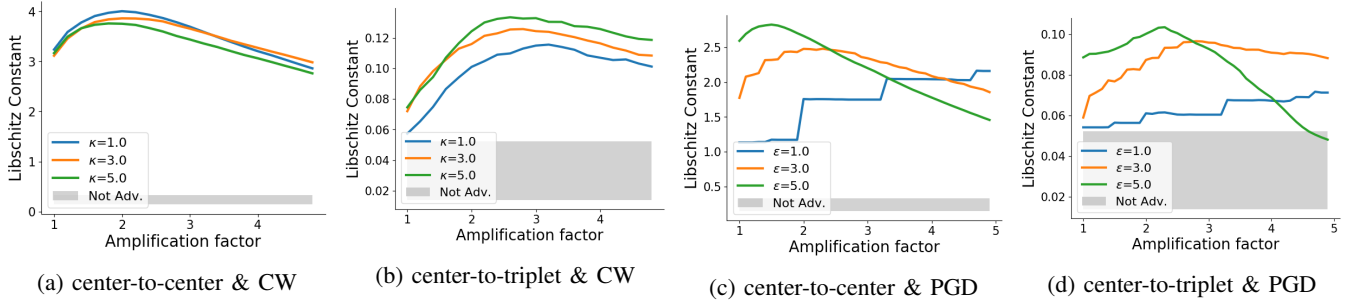


Fig. 3: Lipschitz constant. (a) and (c) represent  $F_\theta$  as the center loss model with CW and PGD attacks, respectively. (b) and (d) show transferability from the center loss to the triplet loss model with the two attacks.

Our aim is to find sub-spaces  $S \subseteq \mathbb{R}^n$  that have high  $L_f(S)$ ; for these sub-spaces, a small perturbation in the image space  $\mathbb{R}^n$  will lead to a high perturbation in the embedding space  $\mathbb{R}^m$ .

Let  $x$  be an image, and  $\mathbb{A}$  be an attack algorithm that for a function  $f$  and input  $x$  outputs a perturbation  $\mathbb{A}(f, x)$  (*i.e.* for intuition sake the reader can think of  $\mathbb{A}$  as typical algorithms for constructing adversarial examples – CW or PGD). Let  $\delta = \mathbb{A}(f, x)$  denote the adversarial perturbation. If  $B(z, \beta)$  represents a ball of radius  $\beta$  with center  $z$ , we observe the following relationship (for moderate size of  $\beta$ ):

$$L_f(B(x, \beta)) < L_f(B(x + \delta, \beta))$$

We believe that amplifying adversarial examples with amplification factor results in the perturbed image lying in the space with *large Lipschitz constant*. Prior work [37] further provides evidence that points with large Lipschitz constant have low robustness.

**Empirical Validation:** We conduct experiments to validate that classifiers exhibits a large Lipschitz constant in the (adversarial) subspaces of the input space. We consider a set of 64 images belonging to the same person and two face recognition architectures, which we name center and triplet. We elaborate further on both classifiers in § VIII. We use both CW and PGD attacks to generate adversarial examples over the center model using different parameters –  $\kappa$  for CW and  $\epsilon$  for PGD (refer to the original papers for more details [6], [17]).

Here, we aim to demonstrate the adversarial examples exhibit larger Lipschitz constants or slopes than non-adversarial examples. In particular, given two input images  $x_1$  and  $x_2$ , we report  $\frac{\|F_\theta(x_1) - F_\theta(x_2)\|_2}{\|x_1 - x_2\|_2}$  where  $F_\theta(\cdot)$  refers to the logits of either the center or triplet model. We consider two cases, the first is where  $x_1$  and  $x_2$  are two unperturbed images of the same person. The second case is where  $x_2 = x_1 + \alpha \cdot \delta$  is an adversarial example generated using either CW or PGD attacks on the center model. Here,  $\alpha \geq 1$  denotes the amplification factor.

We consider four scenarios (refer Fig. 3) computing the slopes over the same center model and the triplet models over both attacks. Fig. 3a shows, as a function of amplification, the slope values of the adversarial examples over different  $\kappa$  values for the CW attack. The gray strip in the plot corresponds to

the range of the slope values for the unperturbed images. Since amplification is inapplicable for unperturbed images (*i.e.*  $\delta = 0$ ), the gray strip is consistent throughout the plot. Similarly, the rest of plots in Fig. 3 show the slopes when (a)  $F_\theta$  is the triplet model with the CW attack (Fig. 3b), (b)  $F_\theta$  is the center model with the PGD attack (Fig. 3c), and (c)  $F_\theta$  is the triplet model with the PGD attack (Fig. 3d). Fig. 3b and Fig. 3d correspond to transferability to a black box model.

**Takeaways:** First, in all cases the slopes corresponding to the adversarial images considerably exceed those of the unperturbed images. Second, amplification of the perturbation increases the slope of the output of the classifier, especially for both the transferability cases. As evident from Fig. 3b and Fig. 3d, the slope increases as we apply amplification. In conclusion, examples in the input spaces of the models seem to be associated with adversarial subspaces that have large Lipschitz constant than space of legitimate examples. The plots of Fig. 3 highlight a sample of those spaces over two models (including one with transferability).

## VI. USER STUDY

We conducted a user study to assess *user-perceived utility* of the images that Face-Off generates. We performed this assessment for samples generated using both CW and PGD attacks. Through this study, we aim to understand the amount of perturbation that users are willing to tolerate. We consider two types of images: 1. *portrait*, where the user is the focus of the image –Fig. 4, and 2. *background*, where the background is the focus of the image, and the user is in the image –Fig. 5.

### Study Highlights:

- 1) Privacy-conscious individuals are willing to tolerate larger perturbation levels for improved privacy.
- 2) For the portrait image, 40% of respondents had no problem in uploading a perturbed image to the social media platform (the exact tolerable perturbation level, however, differed among respondents).
- 3) For the background image, the vast majority of users exhibited tolerance to higher image perturbation.

**Participant Recruitment:** We recruited a total of 167 and 163 Amazon MTurk *master* workers for the portrait and background

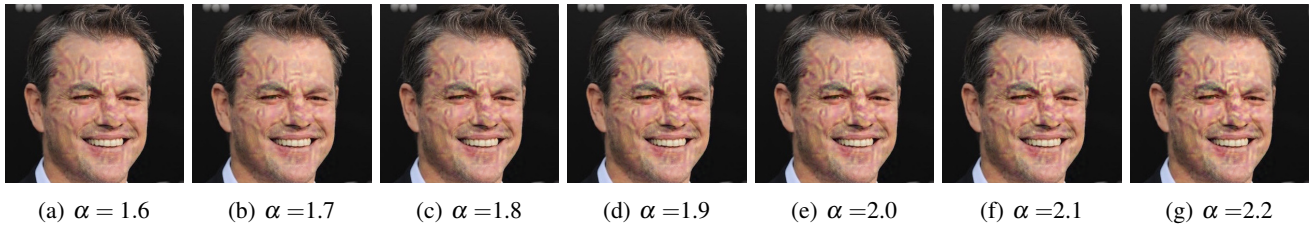


Fig. 4: Photos used in the user study for portrait case with the perturbation increasingly amplified.

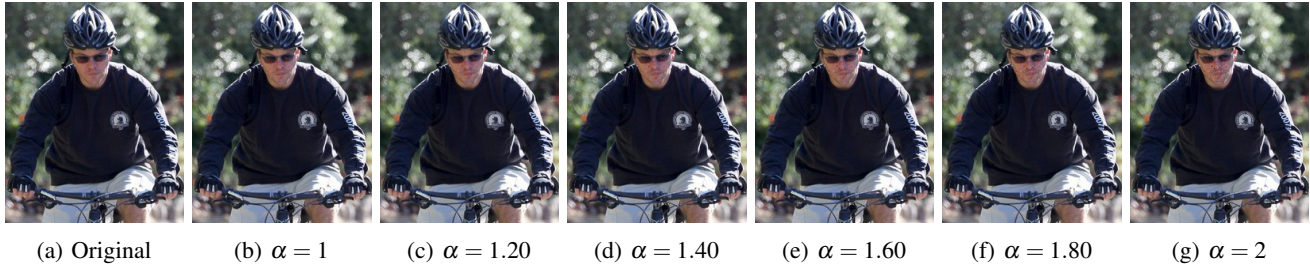


Fig. 5: Photos used in the user study for the background case with the perturbation increasingly amplified. The perturbation is focused on the face region.

TABLE I: Demographics of Participants

Attribute	Portrait	Background
# Workers	167	163
Male	60.1%	68.7%
Female	39.9%	31.3%
Average Age (in years)	37	38
<i>Privacy Preference</i>		
1. Conscious (PC)	75.44%	78%
2. Not Conscious (NPC)	24.56%	22%
<i>Educational Qualification</i>		
1. Some High School	1.19%	1.22%
2. High School	11.97%	10.42%
3. Some College	17.96%	17.79%
4. Associate's	10.17%	9.81%
5. Bachelor's	47.90%	47.85%
6. Graduate	10.77%	12.83%

study, respectively. With this number of users, each image in the portrait study received at least 5 ratings, and each image in the background study received 163 ratings. Each worker was compensated \$1 for their effort, with an average completion time of 6 minutes. We present the demographics of the participants in Table I.

**Study Design:** We used a between-subject design by asking the user to rate a different image every time. For each participant in the portrait group, we display (a) 20 random images (each on a different page) where the amplification factor  $\alpha \in [1.4, 2.4]$ . For participants in the background group, we show the same 20 images where  $\alpha \in [1.4, 2.4]$ . We choose this range as it enables transferability.

After rating the images, we asked the respondents a set of four questions on a 5-point Likert scale to gauge their privacy concern levels. We utilize the ‘‘Concern for Privacy’’ [18] scale

which is modeled after the well-known ‘‘Information Privacy Concern scale’’ of Smith *et al.* [28]. We use this set of questions to divide the respondents into two groups: *Privacy Conscious (PC)* and *Not Privacy Conscious (NPC)*. Respondents belonging to the first group are those who have answered all four questions with either Strongly Agree or Agree. The second group of respondents is those who responded with Neutral, Disagree, or Strongly Disagree any of the questions. Finally, we require the respondents to answer a set of general demographic questions. The respondents were made aware that these questions are optional and require no personally identifiable information.

**Image Evaluation:** For each displayed image, we asked the respondents to answer the following question: ‘‘I have no problem in uploading this photo to Facebook’’ on a 5-point Likert scale. We discuss our observations for the portrait and background scenarios.

*1. Portrait Images:* Each user was shown a set of images with a corresponding  $\alpha$  (randomly chosen from  $[1.4, 2.4]$ ) value unknown to the user. We grouped user responses into 5 buckets corresponding to the ranges  $[1.4, 1.6)$ ,  $[1.6, 1.8)$ ,  $[1.8, 2)$ ,  $[2, 2.2)$ ,  $[2.2, 2.4]$ . These 5 buckets represent increasing levels of perturbation.

We first discuss results for the NPC category (Fig. 6a); as the amplification increases, the number of users who do not wish to upload the image (the strongly disagree category i.e the last column) also increases. The inverse is also true; as the perturbation is lower, the number of participants who wish to upload the image is higher (i.e. the first column). Similar observations can be made for the PC category as well (Fig. 6b). Combining both groups, we found that 40% of the respondents are impartial to uploading at least one of the perturbed images. It is worth noting that portrait images are a unique case, where

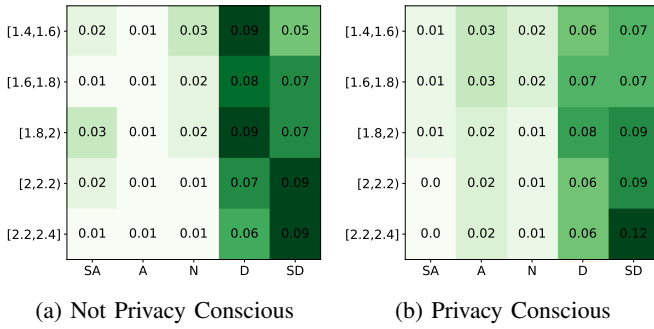


Fig. 6: The distribution of responses for the **portrait** scenario for the privacy conscious and not privacy conscious groups. Each cell value contains the portion of responses for a specific amplification range and user satisfaction value (SA=Strong Agree, A=Agree, N=Neutral, D=Disagree, DA=Strong Disagree).

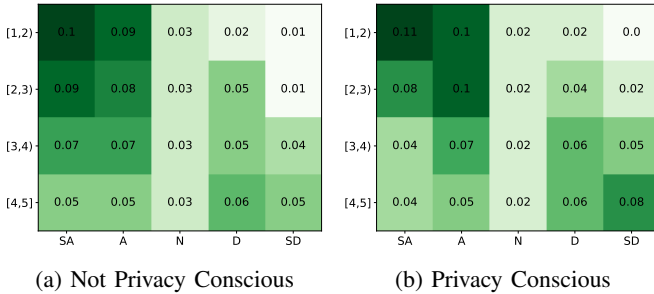


Fig. 7: The distribution of responses for the **background** scenario for the privacy conscious and not privacy conscious groups. Each cell value contains the portion of responses for a specific amplification range and user satisfaction value (SA=Strong Agree, A=Agree, N=Neutral, D=Disagree, DA=Strong Disagree).

the subject is the highlight of these images, with a very limited background context (refer Fig. 16). Thus, the perturbation is more explicitly visible on the user’s face, accounting for the responses received.

Nevertheless, we observe that the PC respondents are slightly more inclined to accept perturbed images than NPC users. This observation is evident from comparing Fig. 6a and Fig. 6b, where the latter figure shows a higher density of responses in the SA-A region. Further, we find the user perception to be dependant on privacy consciousness in all five amplification ranges ( $p < 0.05$  according to the Chi-squared test after applying the Holm-Bonferroni [12] method to correct for multiple comparisons).

2. *Background Images*: Fig. 7 shows the user responses for background images to be far more favorable than the portrait case. As evident from Fig. 5, the user’s face constitutes a small region of such images, with other relevant features. Thus, resizing, amplifying, and adding the adversarial perturbation

does not make as noticeable a difference as in the portrait image case. Except for the last range of amplification values, the vast majority of the respondents agreed to upload the perturbed image to the social media platform. In the first three ranges of amplification, we did not observe privacy consciousness to be a factor in the respondents’ answers ( $p > 0.05$  according to the Chi-squared test after applying the Holm-Bonferroni method to correct for multiple comparisons). In one case, one of the respondents indicated that they do not observe any difference in the images and wondered whether we are “testing” respondents by showing the same image for every question. The only exception was the last amplification range, where large image perturbation is high enough to be unacceptable to our privacy conscious respondents.

Finally, it is clear that the choice of the image exhibits a clear distinction in the user’s perception of the perturbation ( $p = 0$  according to the Chi-squared test when comparing background and portrait responses over the same ranges of amplification). This distinction holds for all, NPC, and PC respondents. Users are typically more interested in preserving their privacy in situations related to a certain activity, behavior, or social context [3]. A portrait image contains little context about a user activity or behavior. On the other hand, background images contain more context related to user activity, behavior, location, and social circles. For these images, users have a high incentive to avoid being automatically tagged and tracked by social media platforms.

The observations from our user study show that Face-Off improves on the privacy-utility trade-off of users. Most of the respondents have no problem in uploading the background and perturbed image, regardless of their privacy stance. Even for portrait images, a part of privacy-conscious respondents accepted uploading perturbed images.

## VII. OFFLINE PARAMETER SELECTION

To determine the parameters needed at runtime, we study the effect of perturbation amplification on transferability using the MNIST [14] and CIFAR-10 [13] classification tasks. For each classification task, we train two networks: the first as a substitute network which we use to generate the adversarial examples, and the second as a black box model on which we test the amplified adversarial example. We trained the substitute models to accept images at a smaller size than the black box model to mimic our application scenario. Once the perturbed example is generated, we resize the perturbation to the image’s original size, add it to the original image. For this section, we report transferability as the portion of examples that are misclassified by the black box model.

We trained two networks for the MNIST classification task: the substitute model is a 6-layer CNN with an image input size of  $20 \times 20$ ; this model has a test accuracy of 99.4%. The black box model is a CNN of a similar structure but accepts input images of size  $28 \times 28$ ; this model has a test accuracy of 99.35%. For the CIFAR-10 task, we trained a 6-layer CNN as a substitute model that accepts input images of size  $20 \times 20$ ; the test accuracy of the model is 72%. The black box for the

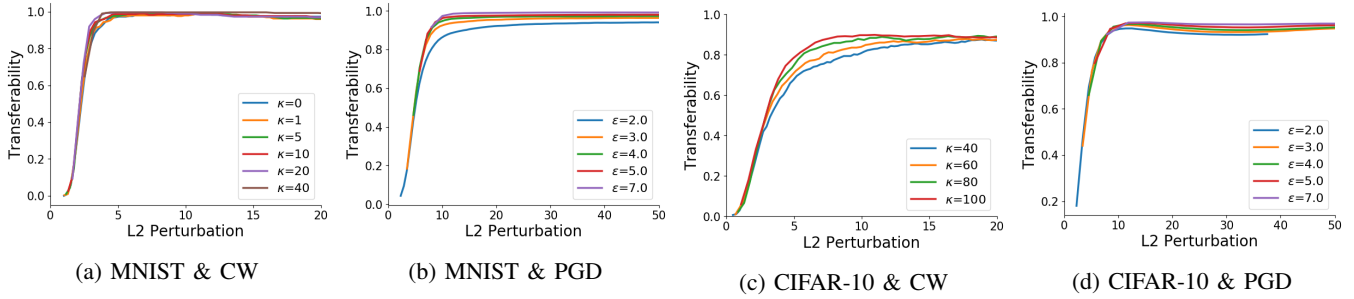


Fig. 8: Transferability to (a) MNIST model with CW attack, (b) MNIST model with PGD attack, (c) CIFAR-10 model with CW attack, (d) CIFAR-10 model with PGD attack.

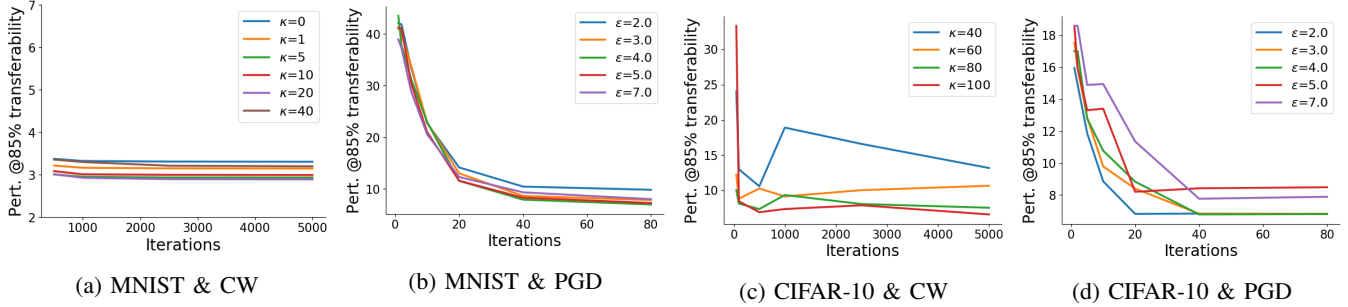


Fig. 9: Perturbation  $\ell_2$ -norm with at least 85% transferability to (a) MNIST model with CW attack, (b) MNIST model with PGD attack, (c) CIFAR-10 model with CW attack, (d) CIFAR-10 model with PGD attack.

CIFAR-10 dataset is VGG-based that accepts inputs of size  $32 \times 32$  and has a test accuracy of 93.59%.

Using the test set of both MNIST and CIFAR-10 tasks, we generate adversarial versions for *each element* of the test set, using two attacks: CW and PGD. For each attack, we varied the number of iterations and the input parameters:  $\kappa$  and  $\varepsilon$  for the CW and PGD attacks, respectively. For the CW attack, we generate an adversarial example of each element in the test set using 72 configurations of  $\kappa$  and number of iterations. For the PGD attack, we generate 84 different versions varying  $\varepsilon$  and the number of iterations. Finally, we amplify the perturbations (in each configuration for both datasets over the CW and PGD attacks) with the amplification factor ( $\alpha$ ) varying between 1 and 25 at 0.25 increments. Our objective in this experiment is two-fold: we aim to study the impact of amplification on transferability, and whether amplification can reduce the runtime of generating the adversarial example.

Fig. 8 and Fig. 9 show the transferability for the datasets over the two attacks. In particular, Fig. 8 shows the transferability for several values of  $\varepsilon$  and  $\kappa$  over the highest number of iterations utilized. For a fair comparison, we plot transferability as a function of the  $\ell_2$ -norm of the perturbation ( $=\|\alpha\delta\|_2$ ). In Fig. 9, we report the minimum  $\ell_2$ -norm of the perturbation required to achieve 85% transferability to the black box model. There are several insights that can be drawn from the plots in both figures regarding amplification and its effect on transferability. We list them below.

1. *Running PGD or CW attacks with a high number of iterations result in adversarial examples that transfer better. However, this is at the expense of increased runtime.* Fig. 9 shows the minimum level of perturbation needed to achieve 85% transferability as a function of the number of iterations. For the MNIST dataset, running PGD or CW attacks at low  $\kappa$  and  $\varepsilon$  and a small number of iterations is enough to achieve high transferability, aided by larger amplification (Fig. 9a and Fig. 9b). For the MNIST dataset and CW attack with parameters  $\kappa = 5$  at 500 iterations is enough to generate the examples that transfer with low amplification. Similarly, for the PGD attack applied on MNIST, at 40 iterations an  $\varepsilon$  value of 4 achieves 85% transferability at a low amplification.

2. *Amplification does improve the transferability for both attacks.* Adversarial examples generated over the substitute model do not transfer directly to the black box model; this observation is evident from transferability at the lowest perturbation in four plots (corresponding to the point of no amplification). In all four plots of Fig. 8, amplification increases transferability at the expense of higher perturbation (and consequently human discernibility). The effect of amplification holds over different parameters of both the CW and PGD attacks for both datasets.

3. *The CW attacks achieve the same degree of transferability at lower amplification than the PGD attack.* This insight can be observed by comparing Fig. 8a with Fig. 8b and Fig. 8c with Fig. 8d. This can be explained through the nature of both



attacks; while the PGD attack searches for any adversarial example within a sphere of radius equal to  $\epsilon$ , the CW attack attempts to find *the shortest distance* to an adversarial example with the lowest perturbation subject to a margin of  $\kappa$ .

4. *Adversarial perturbations, surprisingly, survive image resizing.* In our experiments, we generate the adversarial example on an image of size  $20 \times 20$  for both datasets over both attacks. As evident from Fig. 8, amplified, and resized perturbations transfer to black box models. This observation is critical to the design of Face-Off.

5. *Running attacks with lower margins converge much faster but result in examples with low transferability.* The results of CIFAR-10 dataset emphasize the impact of amplification at reducing the needed number of iterations. In this case, the substitute and black box models are very different and are thus more representative of real-world transferability. In both plots of Fig. 9c and Fig. 9d lower values of  $\kappa$  and  $\epsilon$  achieve 85% transferability for lower perturbation and low number of iterations as compared to using higher number of iterations. For example, in Fig. 9c,  $\kappa=60$  converges faster than higher values. After 50 iterations, amplification achieves 85% transferability at nearly the same perturbation level needed for a higher number of iterations for higher  $\kappa$ . Also, Fig. 9d shows that  $\epsilon=2$  achieves 85% transferability at 20 iterations for the same perturbation needed for higher  $\epsilon$  at a higher number of iterations.

## VIII. IMPLEMENTATION & EVALUATION

The current implementation of Face-Off can generate adversarial examples using two attacks (CW, PGD), using two models (center, triplet), using two loss functions (target, hinge). Here, we study which configurations transfer these adversarial examples to commercial face recognition services - Azure Face API, Amazon Rekognition, and Face++ Cognitive Services.

### A. White box Models

Our white box attack is carried out on two state-of-the-art face verification models - the triplet loss model [25], and center loss face model [36].

More details about Facenet’s architecture are available in the original paper [25]. Facenet generates a 128-dimensional embedding for each input face, and uses the  $\ell_2$ -norm between embeddings for verification. Although Google did not release their trained model to the public, a popular model with 99.65% accuracy on Labeled Faces in the Wild (LFW) dataset is available<sup>6</sup>.

The model (originally created in Caffe) was converted to a Keras implementation to ensure compatibility and consistency. In the center loss face model, the output of the fully connected layer serves as the face embedding, and is of dimension 512. As before,  $\ell_2$ -norm between embeddings is used for verification. The reported validation accuracy on LFW is 99.28%.

### B. Black box Models

All the aforementioned APIs accept two images as input (henceforth referred to as one query). They return a confidence value indicating how similar these images are, and a threshold above which these images are marked the same (*i.e.* the faces match). The Azure API returns confidence values in the range  $[0, 1]$ , and is rate-limited. Amazon Rekognition, on the other hand, returns confidence values in the range  $[0, 100]$ , but only accepts S3 objects as queries. Face++ also returns confidence values in the same range as Amazon, but accepts URLs as queries. While both Azure and Amazon’s APIs have a confidence threshold of 0.5 (and 50 respectively), Face++ has a dynamic threshold based on the input. To ensure a consistent comparison, all confidence scores are normalized to values in  $[0, 1]$ , and the match threshold was chosen as 0.5. We elaborate on this decision in § VIII-C.

We have empirical evidence that our examples also transfer to Google’s image search (Fig. 1). However, the lack of a reverse-image search API from Google makes a systematic evaluation nearly impossible.

### C. Experimental Setup

We chose to design adversarial examples for celebrity faces. This ensures that there are a large number of images (both portrait and background) to be perturbed (henceforth referred to as the subject image), and a large number of images (henceforth referred to as the test image(s)) to compare against to measure transferability.

We evaluate all the aforementioned configurations and observe that the center model and hinge loss combination performs the best. Due to space limitations, we focus our discussion on the examples generated using this configuration. For all the black box models under consideration, each adversarial example is compared against 5 test images of the same person, and we report the average confidence value returned by the APIs. We choose a confidence baseline as 0.5; confidence scores of 0 suggest that the face recognition model could not detect a face.

**Processing Pipeline:** For each subject image, Face-Off first detects and segments the face, resizes it, and obtains its adversarial counterpart. Face-Off extracts the perturbation mask, resizes it, and adds it to the resized subject after amplifying it by  $\alpha$ . Face-Off applies MTCNN [40], a widely used face detector, to crop out all the faces detected from the image. Then the faces are down sized to  $96 \times 96$  and  $112 \times 96$  for Facenet and center loss face model, respectively, using bilinear interpolation available from OpenCV<sup>7</sup>. Note that a bulk of the computational costs rise in the generation of the adversarial example (which we measure in §VIII-G); the process of detection, resizing and amplification are computationally efficient.

**Evaluation Layout:** We first discuss our results for the CW attack, followed by the results for the PGD attack. For both attacks, we measure transferability (*i.e.* if the produced example

<sup>6</sup><https://github.com/davidsandberg/facenet>

<sup>7</sup><https://docs.opencv.org/2.4>

is correctly matched with the test images) across all 3 black box models, as a function of the  $\ell_2$ -norm of the perturbation ( $\|\alpha\delta\|_2$ ). To ensure a fair comparison, all figures are plotted in the same  $[0, 1]$  confidence region. We fix the number of iterations to 500 iterations for the CW attack, and 50 iterations for the PGD attack. We conducted out all experiments between July 25 and August 6, 2018. Across all plots, lower the confidence values, better the privacy gains provided.

We make conservative assumptions about face recognition systems, and comprehensively evaluate the aforementioned transferability metric by comparing (a) cropped adversarial images to a cropped baseline of test images ( $C$  vs  $C$ ), and (b) resized adversarial images against a resized baseline of test images ( $R$  vs  $R$ ). We resume our discussion by relating the user-tolerable amplifications observed in § VI with its corresponding (average)  $\|\alpha\delta\|_2$ ; the  $\ell_2$ -norm of the perturbation is a good indicator of human (im)perceptability, and can act as a proxy for the amplification factor. Thus, results in this section are a function of the  $\ell_2$ -norm. We conclude with measurements of system performance such as ideal number of iterations and wall-clock time required for these iterations.

#### D. Carlini Wagner

The success of the CW attack is reliant on two factors, the margin  $\kappa$ , and the amplification factor  $\alpha$ . Across all experiments described in this subsection, we varied  $\kappa$  in  $[0, 5.8]$  at increments of 0.2, and varied  $\alpha$  from  $[1, 5]$  at increments of 0.1. We do not report all the graphs due to space restrictions.

**Observations:** Across all values of  $\kappa$  considered, the  $R$  vs  $R$  case is the most successful (refer Fig. 10a) *i.e.* the confidence value is always less than 0.5. For the  $C$  vs  $C$  scenario, there is no transferability at lower amplification factors ( $< 1$ ); transferability increases as amplification increases, and we begin to observe transferability at  $\|\alpha\delta\|_2 \approx 6$  (for Azure),  $\|\alpha\delta\|_2 \approx 4.5$  (for Rekognition), and  $\|\alpha\delta\|_2 \approx 12$  (for Face++). We also observe that the slope decreases beyond a specific point across all three models, suggesting that increasing the amplification factor  $\alpha$  will only produce marginal privacy gains. In the magnified region of the plot (*i.e.* the upper half), we observe no correlation between the value of  $\kappa$  and confidence for both the  $R$  vs  $R$  and  $C$  vs  $C$  case. This suggests that the choice of  $\alpha$  is more relevant for transferability than the choice of  $\kappa$ .

#### Insights:

1. The adversarial examples generated using the CW approach transfer to all three black box models under consideration, at the expense of varying levels of  $\|\alpha\delta\|_2$ .
2. For comparable values of  $\alpha$  (and  $\|\alpha\delta\|_2$ ), transferability in the  $R$  vs  $R$  case is better than that in the  $C$  vs  $C$  case across all black box models (refer Fig. 10, 11, and 12). This suggests that the resizing operation further enhances the perturbation in unintuitive ways, an effect we will be exploring in future work.
3. The exact choice of  $\kappa$  does little to impact transferability.
4. Transferability increases with  $\alpha$  and is better in some models

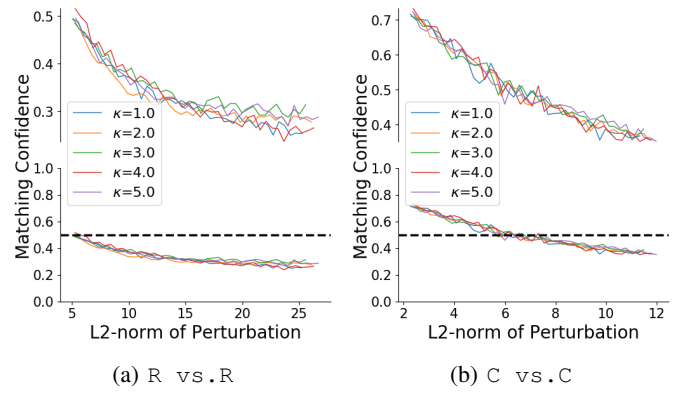


Fig. 10: Transferability to Azure Face API with CW attack.

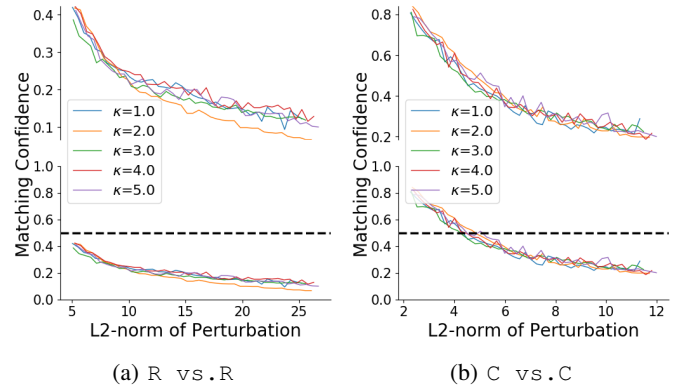


Fig. 11: Transferability to AWS Rekognition API with CW attack.

(Fig. 11a) than others (Fig. 12a). This suggests that some models are closer to our substitute models than others.

#### E. Projected Gradient Descent

The success of the PGD attack relies on two factors,  $\epsilon$ , and the amplification factor  $\alpha$ . Across all experiments described in this subsection, we vary  $\epsilon$  in  $[0, 5.8]$  at increments of 0.2, and vary  $\alpha$  in  $[1, 5]$  at increments of 0.1. The general trend for PGD is the same as that of CW -  $R$  vs  $R$  transfers better than  $C$  vs  $C$ .

**Observations:** Here, the choice of  $\epsilon$  has a greater impact on the rate of transferability (*i.e.* how quickly, in terms of amplification, the example reaches the 0.5 threshold). Larger the value of  $\epsilon$ , faster the transferability (steeper slope), as highlighted across all models. Larger values of  $\epsilon$ , when amplified also crash the face detector (represented by gaps in the plots), a phenomena not observed in the CW scenario. In the  $C$  vs  $C$  case,  $\epsilon = 1$  produces an adversarial example that transfers only when amplified by a large factor (as highlighted by the large  $\|\alpha\delta\|_2$ ). As before, transferability across different models requires different levels of  $\|\alpha\delta\|_2$  (and consequently,  $\alpha$ ).

#### Insights:

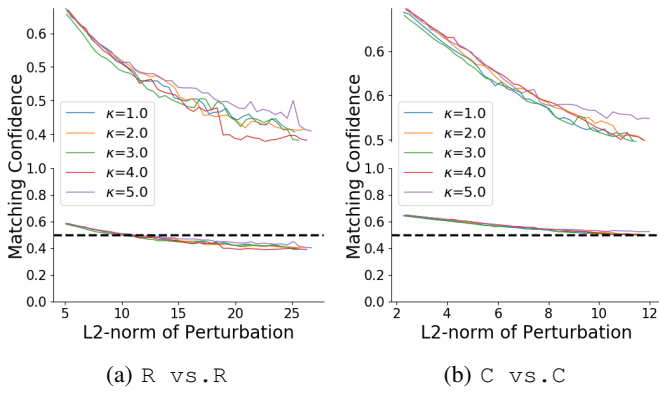


Fig. 12: Transferability to Face++ API with CW attack.

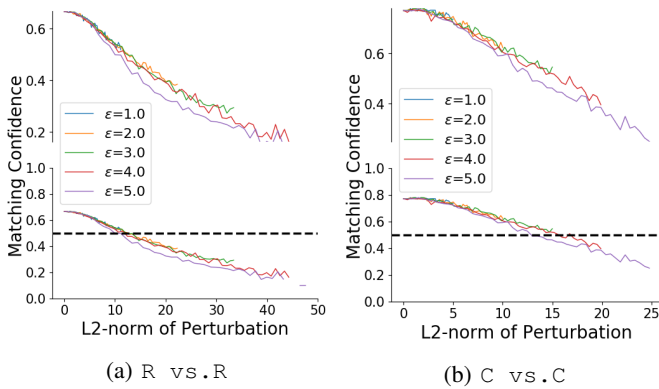


Fig. 13: Transferability to Azure Face API with PGD attack.

1. PGD-generated adversarial examples also transfer across all models. However, they produce far greater perturbation than those produced by the CW attack; CW attempts at minimizing the perturbation, which is not the objective of PGD.
2. Larger values of  $\epsilon$  transfer faster. Hence, the exact value of  $\epsilon$  under consideration is crucial. This is observed in Fig. 13, 14, and 15.

#### F. Interpreting Amplification Factors

In our user study, the MTurk workers were shown images of varying degrees of perturbation (as discussed earlier). A highly perturbed image (with large amplification factor) is one with a large  $\ell_2$ -norm of perturbation, and a less perturbed image is one with a low  $\ell_2$ -norm. We quantify these  $\ell_2$ -norms of perturbation in terms of amplification factors in Fig. 10, 11 and 12. Subsequently, we plot the  $\ell_2$ -norm of the resulting adversarial image ( $\|\alpha\delta\|_2$ ) as a function of amplification.

Fig. 16a and 16b show that transferability occurs at  $\ell_2$ -norm of perturbation larger than 8 for portrait, and larger than 0 for background.

**Takeaway:** The aforementioned ranges correspond to the acceptable amplification factors determined by the user study in § VI.

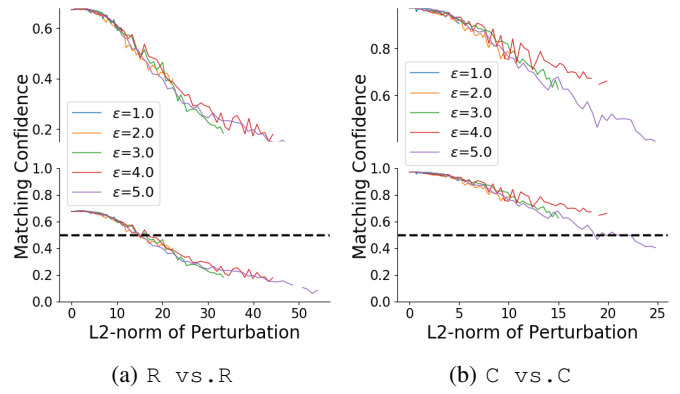


Fig. 14: Transferability to AWS Rekognition API with PGD attack.

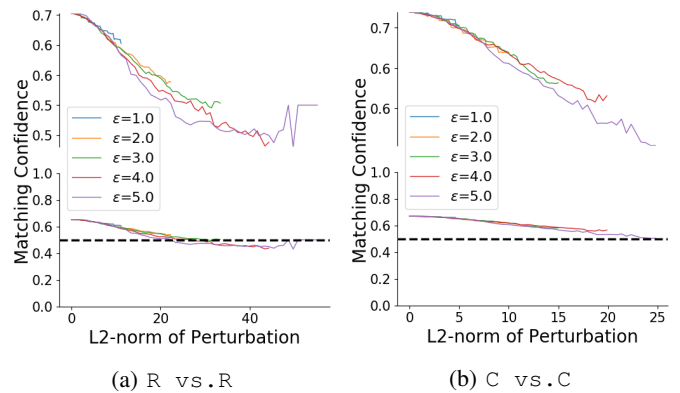


Fig. 15: Transferability to Face++ API with PGD attack.

#### G. Execution Time

Fig. 17 shows the time needed to return an adversarially perturbed face using an Nvidia TITAN Xp GPU (Fig. 17a) and Intel 4.2 GHz Intel Core i7 (Fig. 17b). Face-Off’s center model accepts as input faces of fixed size; the image size does not affect the running time. Rather, the number of iterations and the batch size ( $N$ ) control the time consumption. Both figures (Fig. 17a and Fig. 17b) show the perturbation size (after amplification) that achieves transferability (failed matching) at Azure Face API for each number of iterations and batch size. Those numbers are the same regardless whether the execution happened on GPU or CPU; we show a subset of them at each figure for presentation reasons.

On the GPU (Fig. 17a), for the highest number of iterations and largest batch size, the perturbed image can be generated within 35 seconds. Nevertheless, because of amplification, a lower number of iterations and/or a smaller batch size result in a perturbed face (of similar perturbation size) that transfers to a black box API. In such a case, an adversarial face can be generated in less than 10 seconds per image.

Unsurprisingly, when executed locally on a CPU, Face-Off takes longer to generate an adversarial face. Here, amplification also helps to reduce the time consumption. As evident from

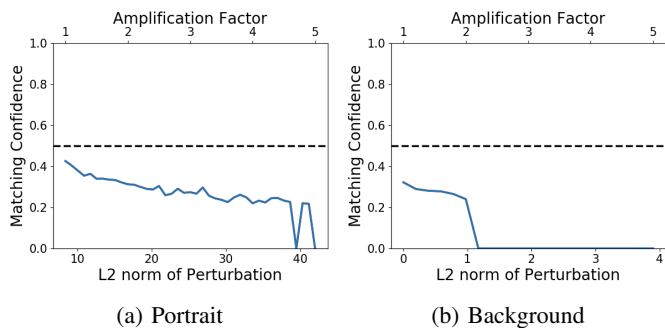


Fig. 16: Relationship between amplification and  $\ell_2$ -norm and their effect on transferability to Azure API. Results correspond to the images used in the user study.

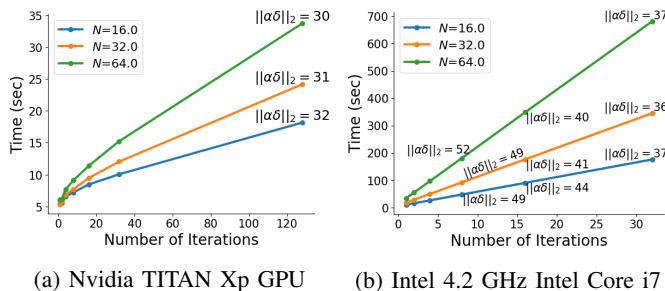


Fig. 17: Time to generate adversarial examples per face using the CW attack  $\kappa=0$ . The text next to some data points indicate the required perturbation size to achieve transferability to Azure Face API.

Fig. 17b, Face-Off can generate an adversarial face with a comparable perturbation size to the best case, within 90 seconds. Depending on the available time budget, the user can tune the privacy/utility trade-off to generate perturbed faces that completely transfer with relatively high perturbation or faces that reduce the social media platform’s confidence with lower perturbation.

## IX. DISCUSSION

We observe that our adversarial examples survive lossy compression at the expense of modest losses in privacy (reduction of matching confidence). In Fig. 18, we plot the difference in confidence values (on the Azure API) between a test image and an adversarial image, when the adversarial image is passed as a PNG (lossless compression) and a JPG (lossy compression). The upper half of the plot are regions where the JPG has lower confidence than the PNG image, and vice-versa. We observe that the magnitude of the difference in confidence values is minimal, suggesting that the choice of compression standard does not impact the results.

*Limitations:* We highlight some limitations of Face-Off, which we hope to address in future work.

- 1) Like other black box attack schemes [33], [16], [29], [20], [21], our approach does not provide guarantees

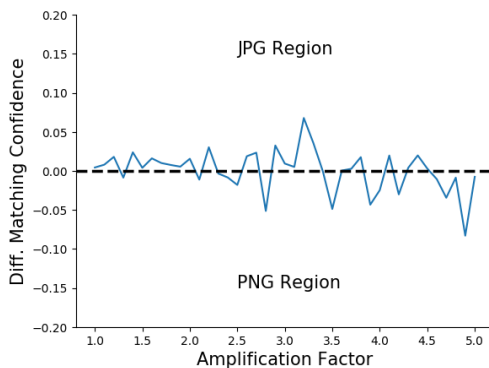


Fig. 18: Adversarial examples survive lossy compression

on transferability. Even with high amplification, the adversarial examples may still not transfer. However, our approach always enhances privacy if privacy were to be measured by the decreasing confidence with which these metric networks are able to match faces. In addition, amplification offers users the flexibility to balance the privacy-utility trade-off; privacy-conscious users can increase amplification and obtain greater privacy, at the expense of more visible perturbation.

- 2) While the time required for generating the adversarial example can potentially bottleneck real-time image upload, we envision alternate deployment strategies, such as offline adversarial example generation to circumvent this bottleneck.
- 3) A scenario that Face-Off cannot circumvent is when other people on social media platforms tag faces.
- 4) The biggest limitation of our work, similar to all other adversarial example generation strategies, is the ever-improving robustness of black box models. Increasing robustness also makes images uploaded earlier at risk of being tagged correctly.
- 5) Unlike the work of Sharif *et al.* [26], we are unaware if the adversarial examples we generate can be transferred to the real-world to preserve visual privacy.

## X. RELATED WORK

### A. Black Box Attacks

As instantiations of earlier attacks, several works demonstrate that some adversarial examples generated for one model may also be misclassified by another model [29], [20], [21]. In [21], the proposed attack strategy is to train a local model (as a substitute for the target black box) using synthetically generated inputs. The target DNN labels these inputs. The adversarial examples generated by the substitute are shown to be likely misclassified by the target DNN as well. The core ethos of this work is to use the black box network as a labeling oracle to generate adversarial examples that *transfer*.

Another line of work do not utilize the black box models for the example generation process *i.e.* the black box model is never queried; work from Moosavi-Dezfooli *et al.* showed the existence of a universal perturbation for each model

which can transfer across different images [19]. Yanpei *et al.* conducted a study of the transferability of different adversarial instance generation strategies applied to different models [33]. The authors also proposed to use an ensemble of multiple models to generate adversarial examples to obtain increased transferability.

### B. Privacy

Prior to our work, initial explorations have been made to utilize adversarial examples for protecting visual privacy. Raval *et al.* developed a perturbation mechanism that jointly optimizes privacy and utility objectives [23]. Focusing on standard image classifiers, the authors formulate game theory problem between an obfuscator and an attacker. The attacker aims to identify visual secrets in the images perturbed by the obfuscator, while the obfuscator perturbs images such that the perturbed images are similar to the original images as well as fool the attacker.

Targeting face recognition systems, Sharif *et al.* developed a physical attack approach [26], [27]. The proposed algorithm first performs an adversarial attack on digital face images and limits the perturbation to an eyeglass frame-shaped area. This is achieved by applying a binary mask on perturbation during the adversarial attack. Then the adversarial perturbation is printed into a pair of physical eyeglasses and can be worn by a person to dodge face detection, or to impersonate others in these face recognition systems. Being able to bring an adversarial attack into the physical world, this approach preserves visual privacy against face recognition.

The work of Bose *et al.* [4] is most similar to ours. However, it targets Faster R-CNN [24] face *detectors*. Given white box access to a face detector, the proposed scheme trains a generator against it for a given image. The generated adversarial perturbation aims to dodge the face detector so that the faces are not detected. This scheme has two primary differences compared to our work: (i) Bose *et al.* attacks face detectors, while we target face recognition. Thus, we are able to preserve the utility of numerous applications built atop face detection and recognition systems. (ii) Their work attacks a white box system, while we extend the attack to black box online face recognition APIs.

## XI. CONCLUSION

In this paper, we tackle the problem of face recognition by designing Face-Off, a framework that obfuscates face images through the use of adversarial perturbations. We propose two new loss functions that fit metric learning systems; these are compatible with both the CW and PGD attack frameworks to produce adversarial examples. Through extensive empirical evaluation, we conclude that a small multiplicative amplification factor ensures greater transferability to several commercial black box models. We observe that, surprisingly, the perturbations produced survive both image resizing and lossy compression. In future work, we hope to extend these *digital* attacks into the physical world and utilize similar

techniques to address the privacy threats from modalities such as video and text.

## REFERENCES

- [1] Shane Ahern, Dean Eckles, Nathaniel S. Good, Simon King, Mor Naaman, and Rahul Nair. 2007. Over-exposed?: Privacy Patterns and Considerations in Online and Mobile Photo Sharing. In *Proceedings of the SIGCHI Conference on Human Factors in Computing Systems (CHI '07)*. ACM, New York, NY, USA, 357–366. DOI: <http://dx.doi.org/10.1145/1240624.1240683>
- [2] Amir Beck and Marc Teboulle. 2009. A fast iterative shrinkage-thresholding algorithm for linear inverse problems. *SIAM journal on imaging sciences* 2, 1 (2009), 183–202.
- [3] Andrew Besmer and Heather Richter Lipford. 2010. Moving Beyond Untagging: Photo Privacy in a Tagged World. In *Proceedings of the SIGCHI Conference on Human Factors in Computing Systems (CHI '10)*. ACM, New York, NY, USA, 1563–1572. DOI: <http://dx.doi.org/10.1145/1753326.1753560>
- [4] Avishek Joey Bose and Parham Aarabi. 2018. Adversarial Attacks on Face Detectors using Neural Net based Constrained Optimization. *arXiv preprint arXiv:1805.12302* (2018).
- [5] Xiaoyu Cao and Neil Zhenqiang Gong. 2017. Mitigating evasion attacks to deep neural networks via region-based classification. In *Proceedings of the 33rd Annual Computer Security Applications Conference*. ACM, 278–287.
- [6] Nicholas Carlini and David Wagner. 2017. Towards evaluating the robustness of neural networks. In *Security and Privacy (SP), 2017 IEEE Symposium on*. IEEE, 39–57.
- [7] Sumit Chopra, Raia Hadsell, and Yann LeCun. 2005. Learning a similarity metric discriminatively, with application to face verification. In *Computer Vision and Pattern Recognition, 2005. CVPR 2005. IEEE Computer Society Conference on*, Vol. 1. IEEE, 539–546.
- [8] Changxing Ding and Dacheng Tao. 2015. Robust face recognition via multimodal deep face representation. *IEEE Transactions on Multimedia* 17, 11 (2015), 2049–2058.
- [9] Ian J Goodfellow, Jonathon Shlens, and Christian Szegedy. 2014. Explaining and harnessing adversarial examples. *arXiv preprint arXiv:1412.6572* (2014).
- [10] Ralph Gross, Latanya Sweeney, Jeffrey Cohn, Fernando De la Torre, and Simon Baker. 2009. Face de-identification. In *Protecting privacy in video surveillance*. Springer, 129–146.
- [11] Raia Hadsell, Sumit Chopra, and Yann LeCun. 2006. Dimensionality reduction by learning an invariant mapping. In *Computer vision and pattern recognition, 2006 IEEE computer society conference on*, Vol. 2. IEEE, 1735–1742.
- [12] Sture Holm. 1979. A Simple Sequentially Rejective Multiple Test Procedure. *Scandinavian Journal of Statistics* 6, 2 (1979), 65–70. <http://www.jstor.org/stable/4615733>
- [13] Alex Krizhevsky and Geoffrey Hinton. 2009. *Learning multiple layers of features from tiny images*. Technical Report. University of Toronto.
- [14] Yann LeCun and Corinna Cortes. 2010. MNIST handwritten digit database. <http://yann.lecun.com/exdb/mnist/>, (2010). <http://yann.lecun.com/exdb/mnist/>
- [15] Weiyang Liu, Yandong Wen, Zhiding Yu, Ming Li, Bhiksha Raj, and Le Song. 2017. Sphereface: Deep hypersphere embedding for face recognition. In *The IEEE Conference on Computer Vision and Pattern Recognition (CVPR)*, Vol. 1.
- [16] Yanpei Liu, Xinyun Chen, Chang Liu, and Dawn Song. 2016. Delving into transferable adversarial examples and black-box attacks. *arXiv preprint arXiv:1611.02770* (2016).
- [17] Aleksander Madry, Aleksandar Makelov, Ludwig Schmidt, Dimitris Tsipras, and Adrian Vladu. 2017. Towards deep learning models resistant to adversarial attacks. *arXiv preprint arXiv:1706.06083* (2017).
- [18] George R. Milne and Mary J. Culnan. 2004. Strategies for reducing online privacy risks: Why consumers read (or don't read) online privacy notices. *Journal of Interactive Marketing* 18, 3 (2004), 15 – 29. DOI: <http://dx.doi.org/https://doi.org/10.1002/dir.20009>
- [19] Seyed-Mohsen Moosavi-Dezfooli, Alhussein Fawzi, Omar Fawzi, and Pascal Frossard. 2017. Universal adversarial perturbations. *arXiv preprint* (2017).
- [20] Nicolas Papernot, Patrick McDaniel, and Ian Goodfellow. 2016a. Transferability in machine learning: from phenomena to black-box attacks using adversarial samples. *arXiv preprint arXiv:1605.07277* (2016).
- [21] Nicolas Papernot, Patrick McDaniel, Ian Goodfellow, Somesh Jha, Z Berkay Celik, and Ananthram Swami. 2016b. Practical black-box attacks against deep learning systems using adversarial examples. *arXiv preprint* (2016).
- [22] Nicolas Papernot, Patrick McDaniel, Somesh Jha, Matt Fredrikson, Z Berkay Celik, and Ananthram Swami. 2016c. The limitations of deep learning in adversarial settings. In *Security and Privacy (EuroS&P), 2016 IEEE European Symposium on*. IEEE, 372–387.
- [23] Nisarg Raval, Ashwin Machanavajjhala, and Landon P Cox. 2017. Protecting visual secrets using adversarial nets. In *2017 IEEE Conference on Computer Vision and Pattern Recognition Workshops (CVPRW)*. IEEE, 1329–1332.
- [24] Shaoqing Ren, Kaiming He, Ross Girshick, and Jian Sun. 2015. Faster r-cnn: Towards real-time object detection with region proposal networks. In *Advances in neural information processing systems*. 91–99.
- [25] Florian Schroff, Dmitry Kalenichenko, and James Philbin. 2015. Facenet: A unified embedding for face recognition and clustering. In *Proceedings of the IEEE conference on computer vision and pattern recognition*. 815–823.
- [26] Mahmood Sharif, Sruti Bhagavatula, Lujo Bauer, and Michael K Reiter. 2016. Accessorize to a crime: Real and stealthy attacks on state-of-the-art face recognition. In *Proceedings of the 2016 ACM SIGSAC Conference on Computer and Communications Security*. ACM, 1528–1540.
- [27] Mahmood Sharif, Sruti Bhagavatula, Lujo Bauer, and Michael K Reiter. 2017. Adversarial Generative Nets: Neural Network Attacks on State-of-the-Art Face Recognition. *arXiv preprint arXiv:1801.00349* (2017).
- [28] H. Jeff Smith, Sandra J. Milberg, and Sandra J. Burke. 1996. Information Privacy: Measuring Individuals' Concerns about Organizational Practices. *MIS Quarterly* 20, 2 (1996), 167–196. <http://www.jstor.org/stable/249477>
- [29] Christian Szegedy, Wojciech Zaremba, Ilya Sutskever, Joan Bruna, Dumitru Erhan, Ian Goodfellow, and Rob Fergus. 2013. Intriguing properties of neural networks. *arXiv preprint arXiv:1312.6199* (2013).
- [30] Yaniv Taigman, Ming Yang, Marc'Aurelio Ranzato, and Lior Wolf. 2014. Deepface: Closing the gap to human-level performance in face verification. In *Proceedings of the IEEE conference on computer vision and pattern recognition*. 1701–1708.
- [31] Techcrunch. Clearview said its facial recognition app was only for law enforcement as it courted private companies. <https://techcrunch.com/2020/02/27/clearview-facial-recognition-private-companies/>. (????).
- [32] Florian Tramèr, Alexey Kurakin, Nicolas Papernot, Dan Boneh, and Patrick McDaniel. 2017. Ensemble adversarial training: Attacks and defenses. *arXiv preprint arXiv:1705.07204* (2017).
- [33] F. Tramèr, N. Papernot, I. Goodfellow, D. Boneh, and P. McDaniel. 2017. The Space of Transferable Adversarial Examples. *ArXiv e-prints* (April 2017).
- [34] Jiang Wang, Yang Song, Thomas Leung, Chuck Rosenberg, Jingbin Wang, James Philbin, Bo Chen, and Ying Wu. 2014. Learning fine-grained image similarity with deep ranking. In *Proceedings of the IEEE Conference on Computer Vision and Pattern Recognition*. 1386–1393.
- [35] Kilian Q Weinberger and Lawrence K Saul. 2009. Distance metric learning for large margin nearest neighbor classification. *Journal of Machine Learning Research* 10, Feb (2009), 207–244.
- [36] Yandong Wen, Kaipeng Zhang, Zhifeng Li, and Yu Qiao. 2016. A discriminative feature learning approach for deep face recognition. In *European Conference on Computer Vision*. Springer, 499–515.
- [37] T. Weng, H. Zhang, P. Chen, J. Yi, D. Su, Y. Gao, C. Hsieh, and L. Daniel. 2018. Evaluating the Robustness of Neural Networks: An Extreme Value Theory Approach. In *ICML*.
- [38] Chaowei Xiao, Bo Li, Jun-Yan Zhu, Warren He, Mingyan Liu, and Dawn Song. 2018. Generating adversarial examples with adversarial networks. *arXiv preprint arXiv:1801.02610* (2018).
- [39] Eric P Xing, Michael I Jordan, Stuart J Russell, and Andrew Y Ng. 2003. Distance metric learning with application to clustering with side-information. In *Advances in neural information processing systems*. 521–528.
- [40] Kaipeng Zhang, Zhanpeng Zhang, Zhifeng Li, and Yu Qiao. 2016. Joint face detection and alignment using multitask cascaded convolutional networks. *IEEE Signal Processing Letters* 23, 10 (2016), 1499–1503.